Pergamon

Planet. Space Sci., Vol. 43, No. 6, pp. 835–842, 1995
Elsevier Science Ltd
Printed in Great Britain
0032–0633/95 $9.50+0.00

0032–0633(95)00067–4

Moon surface thermal characteristics for moon orbiting spacecraft thermal analysis

Giuseppe D. Racca

Future Science Projects, ESA, Directorate of Scientific Programmes, ESTEC Postbus 299, 2200 AG Noordwijk, The Netherlands

Received 8 March 1995; in revised form 16 March 1995; accepted 30 March 1995

Abstract. The thermal characteristics of the lunar surface are of great importance for the calculation of the surface heat flux affecting a lunar orbiting spacecraft. This paper aims to collate the existing information from the literature and systematically arrange the data in a readily usable way. Two simple surface temperature mathematical models are developed, to simulate steady state and transient behaviour. The analytical model results are compared with experimental measurements and good agreement is found. Finally, the problem of the worst cases for the spacecraft thermal analysis is discussed.

Introduction

During the Moon Orbiting Observatory (MORO) Assessment Study (Racca, 1994) it was realized that a considerable effort had to be performed to correctly simulate the Moon surface thermal characteristics for thermal analysis purposes. Although quite some scientific work has been performed in the past on the subject of lunar brightness temperature and thermal characteristics, none was in a form that was readily usable by the thermal engineers. In addition the problem was aggravated by the fact that the thermal design was very much influenced by these thermal characteristics in the case of a low orbiting spacecraft, which may have not been the case for past missions. Considering the general low albedo shown by the Moon surface, the solar energy is largely re-emitted in the infrared spectrum as moonshine. This makes impractical the usual filtering performed by the ratio of solar absorptivity and infrared emissivity of the thermal control surface coatings. On the other hand it was not possible to take large margins in order to compensate for the lunar surface uncertainties, as it is usually done in preliminary thermal assessments. Doing so would have indeed produced a thermally driven spacecraft design.

The aim of this note is to collect the information about the lunar surface temperature and characteristics which may be of interest to the thermal designers and to organize it in a form readily usable for thermal analysis of Moon low orbiting spacecraft. Two lunar surface temperature models have also been derived, for steady-state and transient conditions.

Lunar surface thermal properties

Various parameters are of interest to the spacecraft thermal analyst, notably:

- $\bar{A}$ solar albedo: the ratio of the solar light reflected into all directions to the total incident light
- ε IR emissivity: the ratio of the surface emitted radiation to the black-body emission at the temperature of interest
- k thermal conductivity of the lunar surface
- ρ average density of the lunar surface
- c average thermal capacity of the lunar surface.

These five parameters allow the lunar surface thermal models, described in the following sections, to be derived which in turn may be used to provide the heat input to the orbiting spacecraft.

Solar albedo

The normal solar albedo (ratio at zero phase angle) varies according to the surface materials photometric properties. A low normal albedo of 0.051 in Oceanus Procellarum and 0.176 on the floor of Aristarchus have been measured (Smith and West, 1983), but also more extreme values can be found in the literature. Most of the measurements have taken place from the ground and therefore on the Moon nearside disk only. An interesting compilation has been made recently in the frame of an ESA contract (Thuillier

et al., 1994). The authors have used Earth based measurements by DLR (Neukum *et al.*, 1991) as well as literature studies, to yield a data base of about 300 locations systematically distributed on the lunar nearside, covering the whole surface. They calculated the disk-integrated albedos for each filter band. The resulting albedo values are compared with published disk-integrated measurements in Fig. 1. In order to compute the total solar albedo, the albedo measurements given in Fig. 1 have been approximated by a least square regression straight line, as per the following equation:

$$A(\lambda) = 0.20039\lambda + 0.00624(\pm 0.02088) \quad (1)$$

where λ is the wavelength measured in μm and the term ± 0.02088 is to account for the dispersion of the data. This represents twice the computed standard deviation of the data points with respect to the regression line, leaving, in the wavelength range considered, unchanged curve slope. This is indeed expected to change substantially when the wavelength increases largely above 1 μm. In order to obtain the total solar albedo, equation (1) has to be integrated over the solar spectrum as per equation (2):

$$\bar{A} = \frac{\int_0^\infty A(\lambda)E(\lambda)\,d\lambda}{\int_0^\infty E(\lambda)\,d\lambda} \quad (2)$$

where $E(\lambda)$ is the solar spectral irradiance. The absolute solar irradiance produced by the calibrated data obtained by the instrument SOLSPEC, flown on the *ATLAS I* mission in March 1992 is shown in Fig. 2. This spectrum contains solar irradiance in mW m^{-2} nm^{-1} for a wavelength range from 200 to 2400 nm.

The solar spectrum can be approximated by a black-body spectral irradiance at a temperature varying with the wavelength. The black-body spectral irradiance at a temperature T is expressed by Planck's equation:

$$E(\lambda, T) = \frac{2\pi hc^2}{\lambda^5} \frac{1}{e^{hc/\lambda kT} - 1}. \quad (3)$$

Expression (3) approximates the solar spectrum of Fig. 2 quite closely by varying the black-body temperature with the wavelength. As an example at $\lambda = 240$ nm, $T = 5200$ K, while at $\lambda = 500$ nm, $T = 6000$ K. However, introducing the temperature dependence in equation (2) would result in a solar albedo dependent on temperature. In addition the knowledge of $A(\lambda)$ is restricted to the wavelength range 400–1000 nm, where the black-body temperature can be considered quite constant at a value of about 5800 K.

The integration of equation (2) yields the following value for the total solar albedo:

$$\bar{A} = 0.127 \pm 0.021. \quad (4)$$

Infrared emissivity

The Moon surface temperature has been measured at several locations during the lunar missions. At the *Apollo*

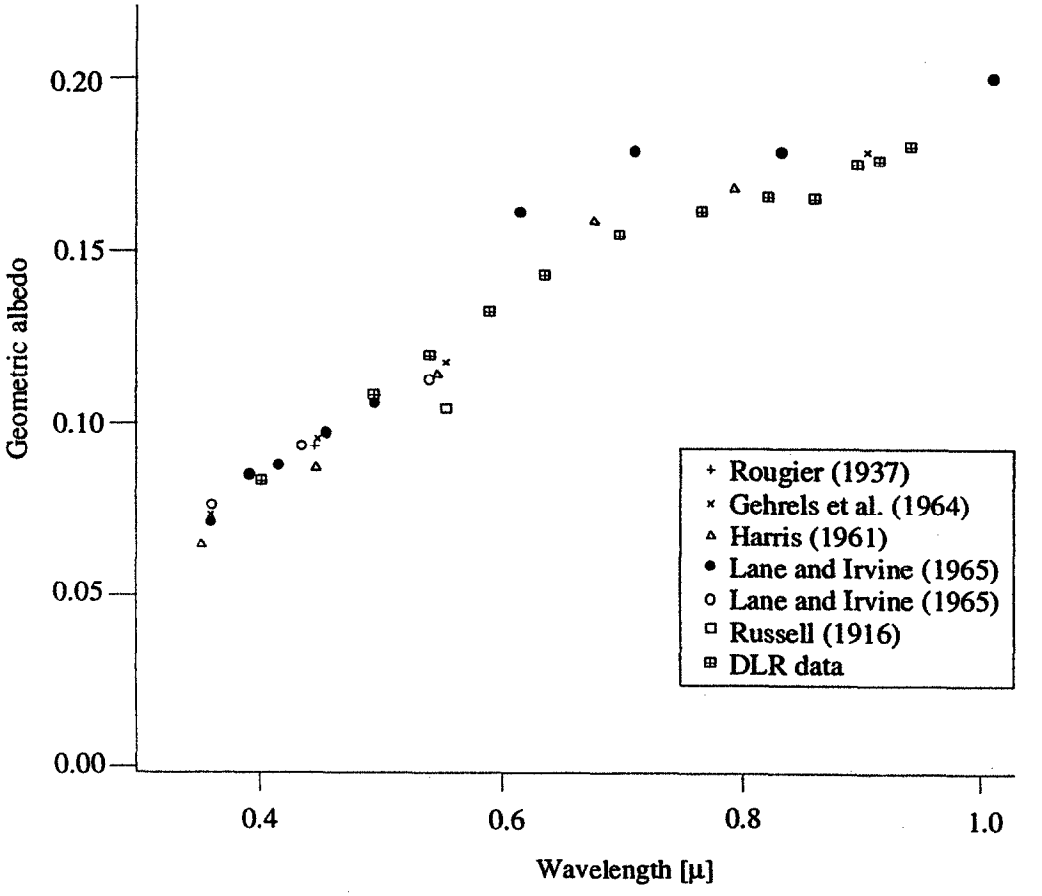

Fig. 1. Disk-integrated albedos versus wavelength (Thuillier *et al.*, 1994)

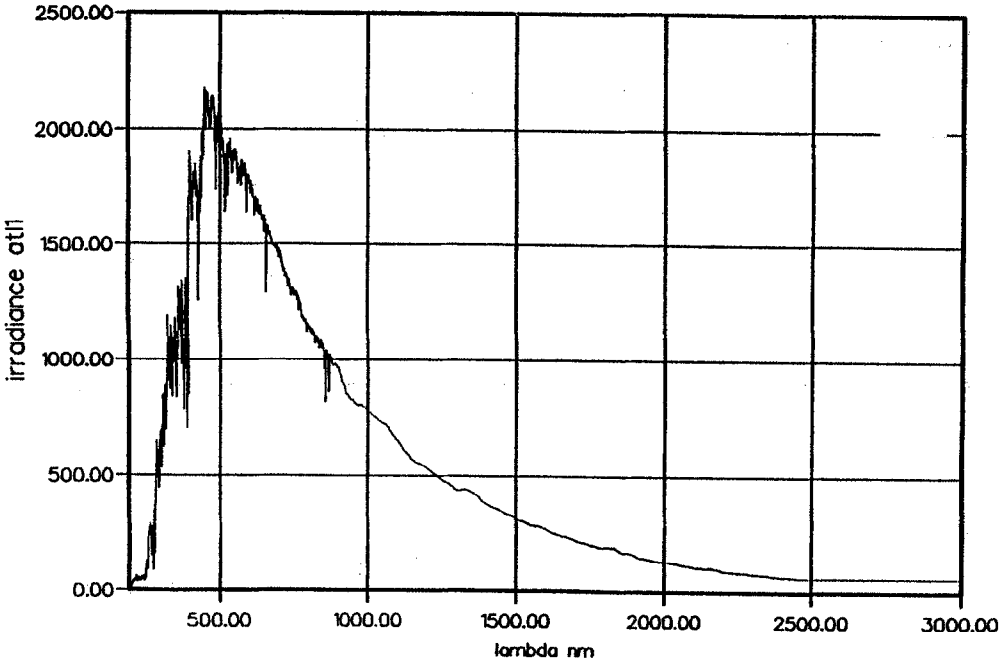

Fig. 2. Absolute solar spectral irradiance from SOLSPEC spectrometer on board *ATLAS I* (Thuillier *et al.*, 1994)

17 site the temperature ranged from 384 K during the day to 102 K just before sunrise. These temperatures correspond to black-body spectrum peaks at 7.5 and 28 μm, in the middle to middle-far infrared range, corresponding to wave numbers of 130–350 cm^{-1}. The lunar surface reflectance data base for this range is quite poor and only few data, based on tests performed on lunar soil samples, have been found in the literature beyond 2.5 μm. The spectral range from 0.3 to 2.5 μm is more studied because of the numerous diagnostic features presented by the reflectance of most of the lunar minerals in this range. In this range the spectral emissivity (equal to the spectral absorptivity = 1 − reflectivity) varies from 0.9 to 0.4. However, some measurements have been performed on *Apollo* 14 and 15 samples in the mid infrared (Logan *et al.*, 1972) and on materials from *Apollo* 11, 12, 14 and 15 in the far infrared (Perry *et al.*, 1972). In the range 7.5–11 μm the emissivity is found (Logan *et al.*, 1972) to be generally higher than 0.9 and approaching unity around a wavelength of 8 μm. The spectral reflectance for wave numbers around 300 cm^{-1} is found varying between 0.15 and 0.10 according to the samples examined (Perry *et al.*, 1972). To simplify the calculations it is necessary to assume a constant value for the surface emissivity in the given range. The above values of infrared emissivity have therefore been averaged and a constant value $\varepsilon = 0.97$ has been considered in the following sections.

Surface density

The surface of the Moon is strongly brecciated and fragmented. This mantle of weakly coherent debris is called regolith. The thickness of the regolith is highly variable from a few metres to 37 m, according to Smith and West (1983). The surface material density has been measured for several samples returned by the *Apollo* missions. The densities vary according to the type of material, from 2.95 g cm^{-3} for fine grained igneous rocks (Type A), to 2.29 g cm^{-3} for the breccia (Type C) and 1.265 g cm^{-3} for the fines (Types D), typically less than 1 cm in diameter (Horai and Simmons, 1972). Smith and West (1983) report a value close to 1 g cm^{-3} for the surface and from 1.5 to 2 g cm^{-3} for a 10–20 cm depth. In the following a conservative (faster thermal response) value for $\rho = 1.3$ g cm^{-3} will be used.

Thermal conductivity

The lunar regolith which covers the lunar surface is an extremely good insulator, particularly very close to the surface. Its thermal conductivity over the first few centimetres has been evaluated (Langseth *et al.*, 1976; Keihm and Langseth, 1975) as close to 10^{-3} W m^{-1} K^{-1}. This means that if a regolith thickness of 10 cm is considered the conductance of the regolith layer would be only 0.01 W m^{-2} K^{-1}. Even for a 100 K difference the heat leak through the regolith layer would only be 1 W m^{-2} compared to the solar constant of about 1400 W m^{-2}. The temperature dependence is not very high, Horai and Simmons (1972) show values varying from 1.7×10^{-3} W m^{-1} K^{-1} at 205 K to 2.4×10^{-3} W m^{-1} K^{-1} at 404 K. A constant value of 2×10^{-3} W m^{-1} K^{-1} will be used in the following.

Thermal capacity

The surface material thermal inertia can be expressed by the thermal parameter as $(k\rho c)^{-1/2}$. Smith and West (1983)

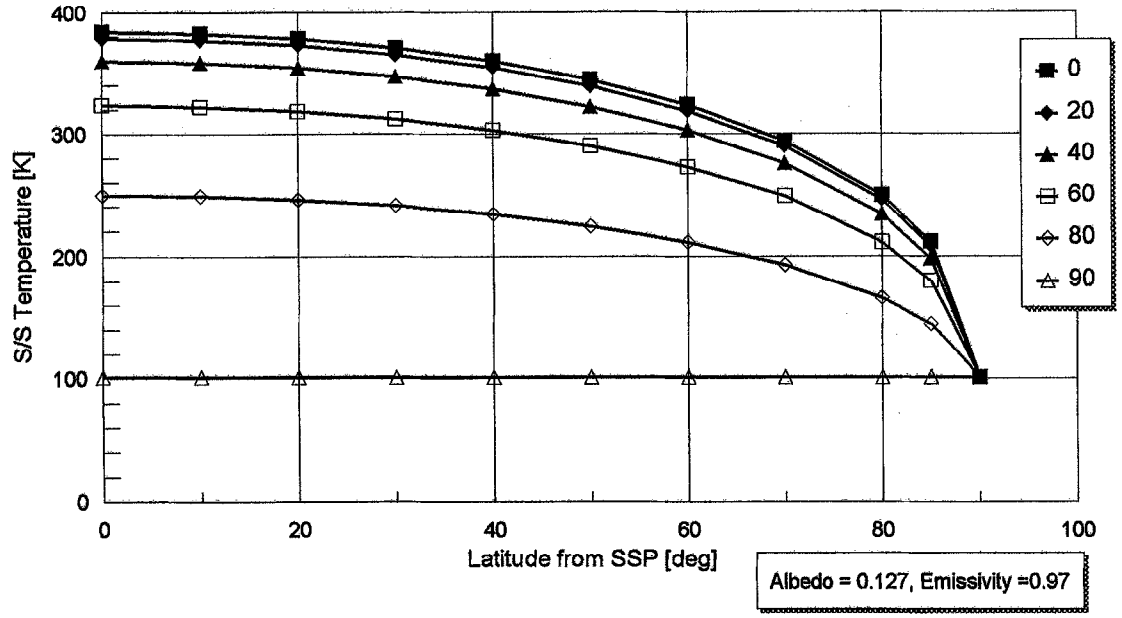

Fig. 3. Steady-state Moon surface temperature, at 1 AU, illuminated side

report a value of the thermal parameter of approximately 800 $cm^2\ s^{1/2}\ K\ cal^{-1}$, which translates into a value for the thermal capacity $c = 1053\ J\ kg^{-1}\ K^{-1}$, if the above thermal conductivity and density are used. The thermal parameter at 300 K has been measured for several types of materials (Horai and Simmons, 1972) and various values have been found: 23.3 $cm^2\ s^{1/2}\ K\ cal^{-1}$ for Type A and 38.9 $cm^2\ s^{1/2}\ K\ cal^{-1}$ for Type C. These are quite different from the Type D material thermal parameter, which has been measured to range between 811 $cm^2\ s^{1/2}\ K\ cal^{-1}$ at 404 K and 1198 $cm^2\ s^{1/2}\ K\ cal^{-1}$ at 205 K. Again a constant conservative value for $c = 800\ J\ kg^{-1}\ K^{-1}$ will be used.

Moon surface temperature model

Using the parameters derived in the above sections, two Moon surface thermal models can be built. The first one is to describe the lunar surface illuminated by the sun at steady-state conditions, i.e. allowing sufficient time for the transient to vanish. This is justified by the length of the lunar day (about 27 days) for most of the lunar surface, both illuminated and shadowed, except in the proximity of the terminators. The second model to be derived is a transient model necessary to describe the surface temperature during the Moon eclipses.

Moon surface steady-state temperature model

Considering a lunar unit surface at latitude ϕ and longitude ψ computed from the subsolar point, a simple energy balance yields the following expression for the steady-state surface temperature:

$$T(\phi,\psi) = \left[\frac{(1-\bar{A})}{\varepsilon}\cos\phi\cos\psi\frac{S_\odot}{\sigma} + \frac{6}{\sigma}\right]^{1/4} \qquad (5)$$

where $\sigma = 5.67\times10^{-8}\ W\ m^{-2}\ K^{-4}$ is the Stefan–Botzmann constant and $S_\odot$ the solar power. A value of 6 W m^{-2} has been introduced as a subsurface cooling flux to reproduce a temperature at sunrise of approximately 100 K, which agrees with the observations, as shown later in Fig. 4. The solar constant (integrated solar irradiance at 1 AU) has been measured (Smith and West, 1983) as $1371\pm5\ W\ m^{-2}$. Taking into account the perihelion and aphelion distances, a variation of $S_\odot$ from 1418 to 1326 W m^{-2} should be considered. On top of these variations, the solar output is also affected by other short-term variations, like solar spots, and long term like the 11-year solar cycle. These variations are in the order of a few tenths of 1% of the solar constant.

Equation (5) is plotted in Fig. 3 for nominal values of $\bar{A}$, ε and $S_\odot$. It can be seen that the maximum temperature at subsolar point (SSP) is about 384 K, while the minimum temperature is found at the poles, and in the whole darkside, at approximately 101 K. It should be noted that as the lunar equator is inclined 1°32′ to the ecliptic plane, the latitude and longitude defined above do not coincide exactly with the selenographic coordinates. However, this difference should be negligible to all practical effects. Caused by this inclination and by the presence of high rims is the presence in the polar regions of permanently shadowed areas. From the recent *Clementine* mission (Shoemaker *et al.*, 1994), an estimated area of 30,000 km^2 within 5° of the south pole remains in shadow in the present phase of precession of the lunar poles. The temperature of that surface is still unknown, since quantitative analysis of the *Clementine* thermal infrared imaging experiment can begin only once the instrument calibration to radiance is completed (Nozette *et al.*, 1994). It is expected that the temperature in those areas will be considerably lower than 100 K. A very recent study (Salvail and Fanale, 1994) predicts a temperature for the crater floors ranging from a minimum of 70 K to a maximum of 120 K.

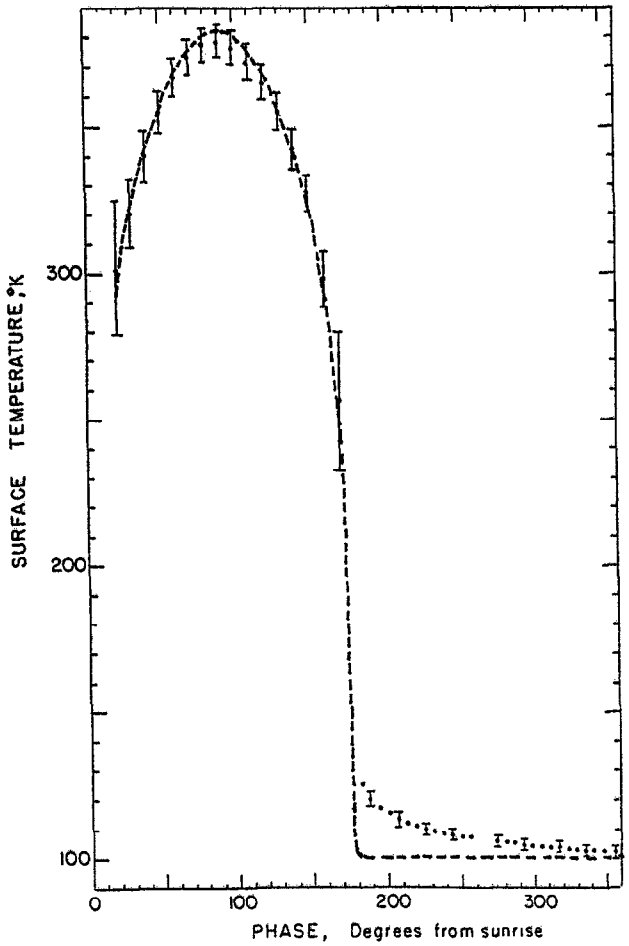

Fig. 4. Surface temperatures at the Taurus Littrow heat flow site (Keihm and Langseth, 1973)

However, the involved area is less than 1/1000 of the whole Moon surface, therefore it is believed that the influence of these regions on an orbiting spacecraft should be completely negligible.

More significant is the surface temperature variation with the uncertainty of albedo as per equation (4) and with respect to the seasonal variation of the solar total irradiance. From equation (5) a variation of ± 2 K at SSP can be found by varying the albedo from 0.106 to 0.148. Similarly, about ± 3 K at SSP is found if the total solar irradiance is varied from 1326 to 1418 W m^{-2}. This model fits quite well with the experimental data, as it is shown in Fig. 4, taken from Keihm and Langseth (1973). The points of Fig. 4 are temperature measurements taken by two thermocouples in the Taurus Littrow heat flow experiment site. The solid vertical bars are estimates of the error limits. The response temperature of the model (5) at a latitude of 20.17°N with an albedo of 0.127 and using a solar total irradiance of 1411 W m^{-2}, corresponding to a December period, is plotted in the same graph with a dash line. The agreement between the model (5) and the measurements is excellent for the whole illuminated side up to 5° from the terminator. The maximum predicted temperature is 381.4 K, while the measured temperature at noon is 384 ± 6 K. The minimum nighttime measured temperature is 102 ± 2 K, while the model provides a minimum of 101.4 K.

For the thermal analysis purposes it should be noted that from equation (5) the higher the albedo the lower the surface temperature. However, this does not mean necessarily that a cold case occurs at high albedo. As a matter of fact the high albedo produces higher radiation from the Moon in the solar spectrum. Therefore, this would result in a cold or hot case according to the thermo-optical properties of the spacecraft surfaces. It should be emphasized that the selected cases should be consistent, therefore high albedo from the Moon has to correspond to a low temperature curve (-2 K at SSP as shown above). The seasonal variations are instead not an uncertainty but rather deterministic values, which have to be considered both for the calculation of the albedo from the Moon and for the surface temperature ($+3$ K at perihelion and -3 K at aphelion at SSP).

Moon surface transient model

The reason for deriving a transient model is essentially to simulate the thermal behaviour of the Moon during the lunar eclipses. A lunar eclipse occurs when the Moon enters either the penumbral or the umbral or both cones of the Earth, as shown in Fig. 5. If only umbral eclipses, either total or partial, are considered, in the period 2001–2005 seven eclipses will take place. The eclipse is total if the entire Moon enters the umbra. The eclipse magnitude is the fraction of the diameter of the lunar disk which is eclipsed at maximum phase, therefore if the magnitude is larger than 1, the eclipse is total. During the considered period the longest eclipse occurs on 28 October 2004. The eclipse timeline has been accurately computed by ESOC (Janin and Castronuovo, 1995) for a hypothetical observer located at the centre of the Moon:

2004.10.28	0:41:08.4	Entry Penumbra
2004.10.28	1:49:52.0	Entry Umbra
2004.10.28	4:20:00.0	Exit Umbra
2004.10.28	5:28:43.5	Exit Penumbra

Since the lunar disk has a finite size, seen from the Earth 0.508°, a portion of it will begin to enter the penumbra cone at some times earlier, i.e. 0.479 h. The portion of the shadowed surface will grow with time with a law which can be quite correctly approximated by a straight line, until the full Moon is in the penumbra shadow. The same will happen when the leading edge of the Moon comes across the umbral edge. This part in turn will exit both the umbra and penumbra cone first. Since the purpose of this analysis is to calculate the thermal conditions of the Moon surface as seen by an orbiting spacecraft, it is important to calculate the overall radiance illuminating the Moon surface during the eclipse. Due to the linear approximation explained above, the total overall solar irradiance can be plotted as in Fig. 6.

During this period the solar energy input varies from a full $S_\odot$ to zero in 2.1 h, stays at zero for 1.54 h and rises again to $S_\odot$ in 2.1 h.

In order to properly simulate the transient, detailed

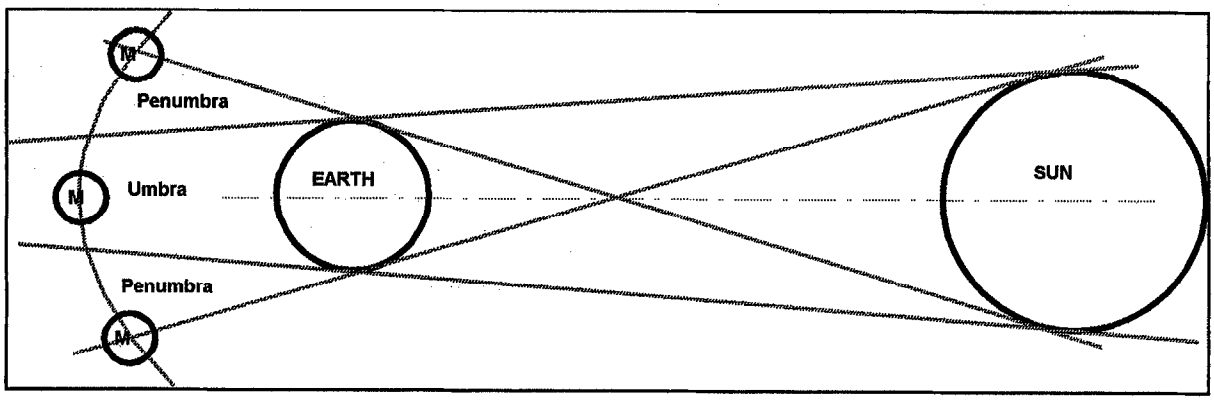

Fig. 5. Lunar eclipse geometry

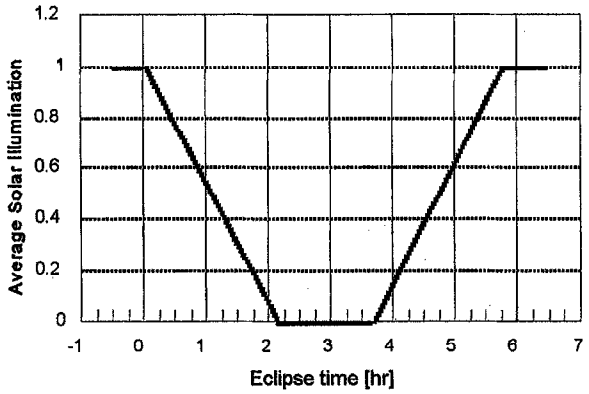

Fig. 6. Total solar irradiance during eclipse

information on the lunar regolith thermal inertia are needed. Alternatively and more simply, one could assume that the surface temperature follows the incoming flux steady-state response with a delay of at most a few minutes, so that during the eclipse basically the same steady-state model (5) would apply, with a linearly varying $S_\odot$. This situation is depicted in Fig. 7, where the thermal transient response is given for five locations on the illuminated side corresponding to ψ and ϕ equal to 0°, 20°, 40°, 60° and 80°.

This model reproduces obviously the 101 K temperature during the complete darkness. This could still be quite a severe environment, especially if the lunar eclipse is preceded and followed by a spacecraft eclipse in its orbit around the Moon. In particular if the spacecraft orbit is close to a twilight orbit, the spacecraft would see very low temperatures for more than 6 h.

If more accurate results have to be found, a better modelling of the surface thermal inertia has to be performed. The regolith layer can be thought of as an isothermal convex very thin two-dimensional slab, with one of the two sides completely insulated and the other side free to radiate to space. The differential equation governing the energy balance in the slab in the absence of an external source is the following:

$$\rho l c \frac{\mathrm{d}T}{\mathrm{d}t} = -\sigma \varepsilon T^4 \tag{6}$$

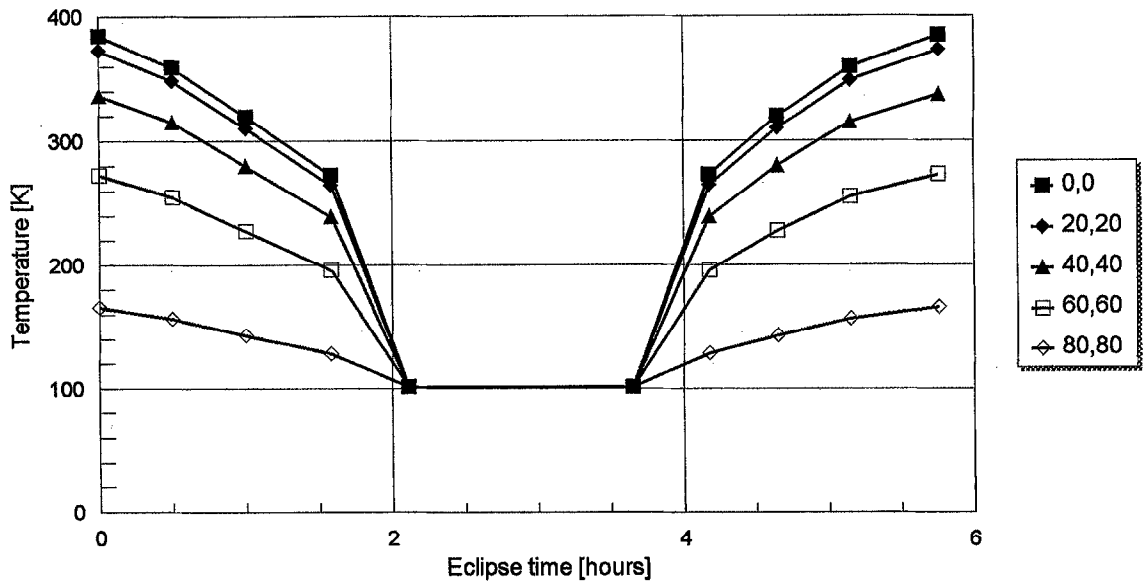

Fig. 7. Moon surface temperature during eclipse, quasi-steady-state thermal transient

where l is the thickness of the regolith and the other parameters are known from before. Integrating equation (6) with the initial conditions that at time $t = 0$, $T = T_0$, the following expression is obtained for $T(t)$:

$$T(t) = \frac{T_0}{\left(1 + \frac{3\sigma\varepsilon}{\rho l c} T_0^3 t\right)^{1/3}}. \quad (7)$$

If $c = 800$ J kg^{-1} K^{-1}, $\rho = 1300$ kg m^{-3}, $\varepsilon = 0.97$, $T_0 = 384$ K and the isothermal regolith thickness $l = 0.1$ m, the temperature transient can be calculated for a given time. Considering the 5.8 h of total duration of the eclipse, the result is $T = 270$ K. Even if in this case the solar input has not been considered for the whole duration of the eclipse, the temperature drop is only about 114 K compared to 283 K that the quasi-steady-state model predicts. Of course model (7) is strongly dependent on the thickness of the isothermal regolith. However, even if the thickness is considered only 1 cm, the temperature would drop only to 142 K after 5.8 h of no external radiation. It seems therefore quite evident that the quasi-steady-state model is too coarse and predicts too extreme values. To further test the above model a comparison has been made with some data of the equatorial brightness temperature after 2 and 4 days after local sunset, from Shorthill (1972). The brightness temperature at the local sunset is 158 K, after 2 days it decreases to 136 K and after 4 days it goes further down to 118 K. Equation (7) reproduces such a behaviour with the above values for c and ρ and considering an isothermal thickness of 19 cm. It seems therefore that considering a thickness of the isothermal regolith of 10 cm is still quite conservative.

A correction is proposed to the quasi-steady-state model: when the solar total irradiance reduces to 1/4 of its value (i.e. after 1.58 h in our model) the sun is switched off and the transient model of equation (7) is plugged in until again the sun illuminates the scene with 1/4 of its value, at this point the quasi-steady-state model is used again with the varying intensity of the solar irradiance. Figure 8 shows the results of the corrected model with an assumed isothermal regolith thickness of 10 cm. It can be seen from the graph that most of the Moon surface would stay well above 200 K, except the high latitude or longitudes which are anyhow already at low temperature even in the presence of the sun. The temperatures shown in Fig. 8 are believed to be more realistic and it is suggested that the spacecraft thermal analyses for the lunar eclipse case are based on those values.

Discussion

The steady-state conditions of the lunar surface are considered to be described with sufficient reliability by equation (5) as plotted in Fig. 3. Seasonal variations of the total irradiance have to be considered to define hot and cold cases. The uncertainty in the albedo should be considered, as explained in an earlier section, in the sensitivity analysis by adding ± 2 K to the values of Fig. 3, however the modified value of the Moon brightness temperature should be used consistently together with the corresponding albedo value and the worst case identified. In case of a polar orbit spacecraft, the orbit tracks follow meridians defined by a longitude value. Therefore in Fig. 3, the curve denoted longitude 0° gives the temperature of the sub-satellite surface points along a noon–midnight orbit, while the curve denoted longitude 90° gives the temperature of the sub-satellite surface points along a so-called twilight or dawn–dusk orbit, constant at 101 K in this approximation. The incoming flux from the Moon surface is produced by the temperature of the whole lunar surface comprised in the view factor of the considered spacecraft surface. Therefore, also in the twilight orbits there will be a radiation contribution coming also from warmer areas, though weighted by Lambert's cosine law. In the most general mission case the situation of the spacecraft orbit can be either a noon–midnight or dawn–dusk or any intermediate position.

The eclipse case defined in the above analysis should be considered for both power and thermal analyses. The

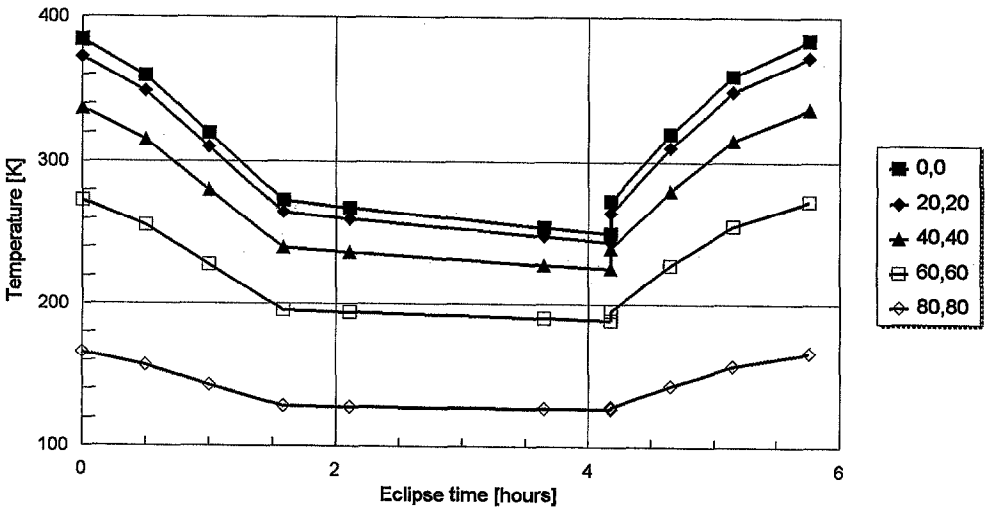

Fig. 8. Moon surface temperature during eclipse with corrected transient model

position of the orbit plane during the eclipse cannot be determined now and it would impose an excessive constraint to the launch window if it was forced to a certain position. In addition this could be done only for one eclipse case and, although the above is the eclipse design case, there are four other total umbral eclipses in the period 2001–2005. It has therefore to be assumed that during the eclipse the plane of the orbit is either perpendicular to the line Sun–Earth–Moon or parallel to it or in an intermediate position. The extreme starting conditions of the lunar surface are therefore given by the extreme curves of Fig. 3. Two extreme cases can be defined: twilight orbit and noon–midnight orbit. In the noon–midnight case the eclipse could possibly occur just after having had an orbital eclipse of 46′ duration (spacecraft occultation by the Moon). This situation would make the total eclipse case of Fig. 6 extending 46′ backwards and 9′ afterwards (total eclipse penumbra and umbra included is 5.758 h = 345′, the orbital period is 118′, therefore during the eclipse we have two complete orbital periods plus 109′ of the third orbit). However, this situation can be avoided by slightly changing the orbital period of the spacecraft by small semi-major axis changes. For example it could be obtained that the eclipse starts just after having had a full sun phase, and finishes when still 9′ of sun are occurring before the next orbital eclipse. Since the times of the eclipse events are well known the orbital manoeuvres could be planned in advance and therefore the best situation from the thermal and power point of view could be selected. The analysis should then concentrate on these cases. The Moon thermal input is given by the curves of Fig. 8.

During the twilight orbits the situation is different, and there are no manoeuvres which can be considered to change the orbit plane. This case should be analysed also using the thermal input of the Moon surface from Fig. 8, lowest curves, which is probably quite negligible. The solar input during the eclipse should be used from Fig. 6, preceded and followed by full sun.

Acknowledgements. The author wishes to thank Harald Hoffmann of DLR, Berlin for providing useful documentation on the solar albedo data, Yves Langevin of IAS, Orsay, member of the MORO Science Team, and Philippe Poinas of ESTEC-YCT, Noordwijk, member of the MORO Engineering Team, for their useful comments and suggestions in reviewing the draft paper. My thanks also to Costanzo Federico of University of Perugia, who refereed the article and provided me with essential recommendations.

References

Horai, K. and Simmons, G., Thermal property measurements on lunar material returned by Apollo 11 and 12 missions, in *Thermal Characteristics of the Moon* (edited by J. W. Lucas), Progress in Astronautics and Aeronautics, Vol. 28. MIT Press, Massachusetts, 1972.

Janin, G. and Castronuovo, M., ESOC Internal Memorandum 95033ESC0018, 2 February 1995.

Keihm, S. J. and Langseth, M. G., Surface brightness temperatures of the Apollo 17 heat flow site: thermal conductivity of the upper 15 cm of regolith. *Proc. Lunar Sci. Conf. 4th*, pp. 2503–2513, 1973.

Keihm, S. J. and Langseth, M. G., Lunar microwave brightness temperature observations reevaluated in the light of Apollo program findings. *Icarus* **24,** 211–230, 1975.

Langseth, M. G., Keihm, S. J. and Peters, K., Revised lunar heat flow values. *Proc. Lunar Sci. Conf. 7th*, pp. 3143–3171, 1976.

Logan, L. M., Hunt, G. R., Balsamo, S. R. and Salisbury, J. W., Midinfrared emission spectra of Apollo 14 and 15 soils and remote compositional mapping of the moon. *Proc. Lunar Sci. Conf. 3rd*, pp. 3069–3076, 1972.

Neukum, G., Jaumann, R., Hoffmann, H., Oberst, J., Wagner, R., Regner, P., Rebhan, H., Hiesinger, H. and Dummel, A., Earth-based multispectral observations of the Moon. *XXII Lunar and Planetary Science Conf.*, U.S.A., Book of abstracts, Part 2, p. 971, March 1991.

Nozette, S., Rustan, P., Pleasance, L. P., Horan, D. M., Regeon, P., Shoemaker, E. M., Spudis, P. D., Acton, C. H., Baker, D. N., Blamont, J. E., Buratti, B. J., Corson, M. P., Davies, M. E., Duxbury, T. C., Eliason, E. M., Jakosky, B. M., Kordas, J. F., Lewis, I. T., Lichtenberg, C. L., Lucey, P. G., Malaret, E., Massie, M. A., Resnick, J. H., Rollins, C. J., Park, H. S., McEwen, A. S., Priest, R. E., Pieters, C. M., Reisse, R. A., Robinson, M. S., Smith, D. E., Sorenson, T. C., Vorder Breugge, R. W. and Zuber, M. T., The Clementine mission to the Moon: scientific overview. *Science* **266,** 1835–1839, 1994.

Perry, C. H., Agrawal, D. K., Anastassakis, E., Lowndes, R. P. and Tornberg, N. E., Far infrared and Raman spectroscopic investigations of lunar materials from Apollo 11, 12, 14 and 15. *Proc. Lunar Sci. Conf. 3rd*, pp. 3077–3095, 1972.

Racca, G. D. (ed.), MORO Assessment Study Technical Report, ESA/ESTEC PF/TR/0934, Noordwijk, The Netherlands, June 1994.

Salvail, J. R. and Fanale, F. P., Near-surface ice on Mercury and on the Moon: a topographic thermal model. *Icarus* **111,** 441–455, 1994.

Shoemaker, E. M., Robinson, M. S. and Eliason, E. M., The south pole region of the Moon as seen by Clementine. *Science* **266,** 1851–1854, 1994.

Shorthill, R. W., The infrared Moon: a review, in *Thermal Characteristics of the Moon* (edited by J. W. Lucas), Progress in Astronautics and Aeronautics, Vol. 28. MIT Press, Massachusetts, 1972.

Smith, R. E. and West, G. S. (eds), Space and Planetary Environment Criteria Guidelines for Use in Space Vehicle Development, NASA TM 82478, MSFC, Alabama, January 1983.

Thuillier, G., Jaumann, R., Mottola, S., Vuorilehto, A. and Korpela, S., Study on the Sun and Moon as Radiation Calibration Targets, ESTEC contract No. 10346/93/NL/CN, June 1994.